Letter

Measurement of work and heat in the classical and quantum regimes

P. Solinas,[1,2] M. Amico,[3,*] and N. Zanghì[1,2]

[1]*Dipartimento di Fisica, Università di Genova, via Dodecaneso 33, I-16146 Genova, Italy*

[2]*INFN - Sezione di Genova, via Dodecaneso 33, I-16146 Genova, Italy*

[3]*The Graduate School and University Center, The City University of New York, New York, New York 10016, USA*

(Received 29 January 2021; accepted 16 June 2021; published 30 June 2021)

Despite the increasing interest, the research field which studies the concepts of work and heat at the quantum level has suffered from two main drawbacks: first, the difficulty to properly define and measure the work, heat, and internal energy variation in a quantum system and, second, the lack of experiments. Here, we report a full characterization of the dissipated heat, work, and internal energy variation in a two-level quantum system interacting with an engineered environment. We use the IBMQ quantum computer to implement the driven system's dynamics in a dissipative environment. The experimental data allow us to construct quasiprobability distribution functions from which we recover the correct averages of work, heat, and internal energy variation in the dissipative processes. Interestingly, by increasing the environment coupling strength, we observe a reduction of the pure quantum features of the energy exchange processes that we interpret as the emergence of the classical limit. This makes the present approach a privileged tool to study, understand, and exploit quantum effects in energy exchanges.

DOI: 10.1103/PhysRevA.103.L060202

I. INTRODUCTION

The oddities of quantum mechanics such as particle entanglement, superposition of states, interference between evolution paths, and so on have proven to be a valuable asset to envision quantum devices able to outperform the corresponding classical ones. From metrology [1] to the detection of gravitational waves [2] passing through quantum computation and communication [3], the exploitation of quantum effects has given a decisive impulse towards new discoveries. With the advent of quantum technologies, this trend will be reinforced, allowing for mass production of quantum-based devices. In this direction, studying the energy exchange processes of a quantum system with an external drive and an environment could have important implications for future developments. This is the aim of a relatively new area of research referred to as quantum thermodynamics.

Although numerous results have been obtained, there is still no clear consensus about how to determine what is the work and the heat in a quantum system [4–9]. In a closed quantum system, the work done on the system is equal to the *variation* of the internal energy of the system. However, the need for information at different times makes it impossible to envision a proper measurement protocol for these quantities [10].

This limitation has delayed experimental verification, especially in the case of a quantum system undergoing dissipative dynamics. Indeed, apart from a single experiment with closed quantum systems [11] and open ones [12–20], a full and convincing measurement of the dissipated heat is still missing. In this Letter, we fill this gap by showing that it is possible to obtain the correct and expected average values of work, heat, and internal energy variation, and important information about the underlying quantum processes.

To avoid any confusion and interpretative pitfalls, we choose a more practical approach by focusing on simple and precise questions. Given a quantum system controlled by an external time-dependent field, how much energy does the system absorb during the evolution? How much work does the external field do on the quantum system? And what is the heat dissipated by the quantum system?

To answer these questions, we implement the detection scheme proposed in Refs. [8,9,21] on an IBMQ device [22]. In particular, we study a two-level quantum system, i.e., a qubit, subject to an external driving field and interacting with an engineered environment. The quantum detector and the engineered environment are represented by three additional qubits. The advantage of using an engineered environment is that we can tune the system-environment coupling strength and explore different dissipative regimes. We implement the scheme on real physical qubits made available in the IBM quantum experience initiative.

Our physical observable is the phase of the detector qubit that is measured with standard techniques (see [22] and the Supplemental Material [23]) from which we recover the information about the average work, heat, and internal energy variation while preserving the full quantum features of the evolution (see [8,9,21] and the Supplemental Material [23]).

Furthermore, from the measured detector phase, we are able to construct a quasicharacteristic generating function and a quasiprobability density function (QPDF) for these physical observables. The QPDF reproduces the statistics of the two-measurement protocol (TMP) [4] when the system is initially in an eigenstate of the Hamiltonian and keeps much more information about the evolution of the system. In a direct

*Present address: Q-CTRL, Sydney, NSW Australia & Los Angeles, California 90013, USA.

analogy with the Wigner function [24], the negative regions of the derived QPDF are associated to the violation of the Leggett-Garg inequalities and are the signature of a pure quantum phenomenon [21,25–28]. The disappearance of these regions in the presence of strong dissipation can be seen as a proof of the emergence of the classical limit in energy exchange processes induced by the presence of an environment.

II. SYSTEM AND DYNAMICS DESCRIPTION

We start by considering a two-level system (denoted by S) that evolves under unitary evolution $U_S = U_z U_x$, with $U_z = \exp(-i\beta\sigma_z)$ and $U_x = \exp(-i\alpha\sigma_x)$ where σ_i $(i = x, y, z)$ are the usual Pauli operators. The system is initially in the state $|\psi_0\rangle = \cos\frac{\theta}{2}|0\rangle_S + \sin\frac{\theta}{2}e^{i\phi}|1\rangle_S$, where $|0\rangle_S$ and $|1\rangle_S$ are the eigenstates of σ_z.

This evolution is generated by the time-dependent Hamiltonian $H_S = \epsilon\sigma_x/2$ for $0 \leqslant t < t_1$ and $H_S = \epsilon\sigma_z/2$ for $t_1 < t \leqslant \mathcal{T}$ with appropriate t_1 and $\mathcal{T}$. The fact that the Hamiltonian changes in time assures that the external field does work on the system [8].

The detector is represented by an additional two-level system (denoted by D). Its Hamiltonian is $H_D = \omega\Sigma_z/2$ (where the operators Σ_i with $i = x, y, z$ are the Pauli operators acting on the detector) and it is time independent. The detector is initialized in an equal superposition of eigenstates of H_D, i.e., $(|0\rangle_D + |1\rangle_D)/\sqrt{2}$.

The coupling Hamiltonian $H_{SD} = f(\chi, t)H_S(t) \otimes H_D$ allows us to store information about the system energy into the accumulated phase of the detector [9,21]. The function $f(\chi, t)$ in H_{SD} determines the time at which the system-detector coupling is active and its coupling strength χ. If the system-detector coupling occurs on timescales much smaller than all of the other timescales, we can assume that $f(\chi, t_i) = \chi/\epsilon\,\delta(t - t_i)$, which generates the transformation $U_{\chi,t_i} = \exp\{i\frac{\chi}{\epsilon}H_S(t_i) \otimes H_D\}$. In particular, in relation the system dynamics described above, we have $U_{\pm\chi,x} = \exp\{\pm i\frac{\chi}{\epsilon}\sigma_x \otimes H_D\}$ and $U_{\pm\chi,z} = \exp\{\pm i\frac{\chi}{\epsilon}\sigma_z \otimes H_D\}$.

We model the dissipation as an amplitude-damping channel [3,29] in which the environment induces relaxation from the excited to the ground state with probability p (see the Supplemental Material [23]). The parameter p determines the strength of the dissipation process and it ranges from $p = 0$, i.e., no dissipation, to $p = 1$, i.e., complete relaxation to the ground state.

If the relaxation occurs in the $\{|0\rangle, |1\rangle\}$, i.e., the σ_z, basis, this corresponds to the transformation

$$\begin{aligned} |00\rangle &\to |00\rangle, \\ |10\rangle &\to \sqrt{1-p}\,|10\rangle + \sqrt{p}\,|01\rangle, \end{aligned} \tag{1}$$

where the first and the second qubits represent the system and the environment, respectively. Physically, this describes the emission of an energy quantum from the system, i.e., the relaxation, and the corresponding absorption from the environment. We assume that the environment is at temperature T and that $k_B T \ll \epsilon$ (where k_B is the Boltzmann constant) so that the processes in which the system is excited by the interaction with the environment are exponentially suppressed and are neglected in Eq. (1). The logical operator that mimics the transformation (1) is denoted as R_z (see Fig. 1 and the Supplemental Material [23]). When the relaxation occurs in the σ_x basis, i.e., during the first part of the evolution, the transformation is analogous to (1) and is implemented with a similar operator denoted by the R_x operator (see the Supplemental Material [23]).

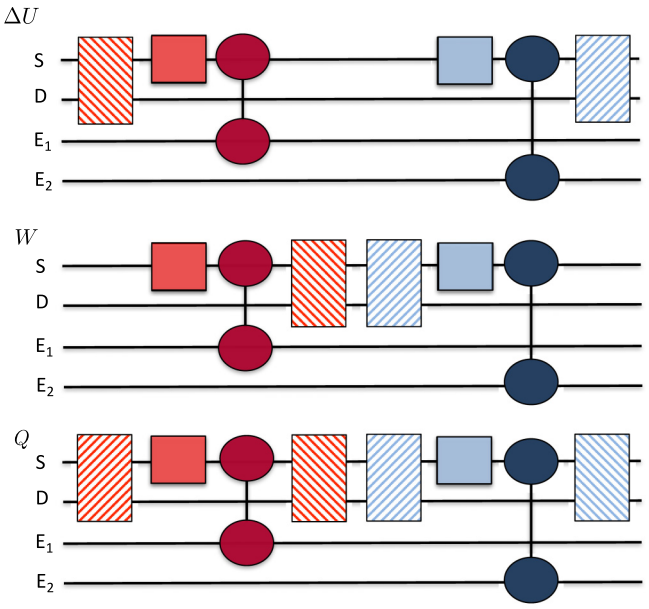

FIG. 1. Three schemes for the detection of the variation of internal energy ΔU, work W, and dissipated heat Q. The letters S, D, E_1, and E_2 denote the system, the detector, and the environment qubits 1 and 2, respectively. The unitary dynamics are represented with red and light-blue filled squares corresponding to U_x and U_z, respectively. The dissipative gates are represented with circles connecting the S qubit with the E_1 and E_2 qubits. They correspond to R_x (dark red) and R_z (dark blue). The system-detector coupling operations are represented with rectangles spanning the S-D qubit space. They are $U_{-\chi,x}$ and $U_{\chi,x}$ (see main text for the definition) represented with dashed red lines from up-left to down-right and up-right to down-left, respectively. The operators $U_{-\chi,z}$ and $U_{\chi,z}$ (see main text for the definition) are represented with dashed blue lines from up-left to down-right and up-right to down-left, respectively. To simplify the presentation, the gates needed to initialize the system and the detector are not shown (see the Supplemental Material [23] for details).

To realize the effect of this engineered environment with the R_x and R_z operators (see Fig. 1), we need two additional two-level systems. On a noisy intermediate-scale quantum (NISQ) device, this translates into two additional qubits (see the Supplemental Material [23]).

In addition, we assume that the unitary evolution occurs on shorter timescales with respect to the relaxation timescale. Hence, we can imagine the system evolution as a sequence of unitary dynamics followed by relaxation.

The building block of the measurement schemes is the operator sequence $U_{\chi,t_i}\,U\,U_{-\chi,t_j}$, where U is a unitary operator acting on the system. As discussed in Ref. [9], this allows us to have information about the *system energy changes in the time interval* $t_i - t_j$. Here, it is of fundamental importance to note that work and heat are associated to different kinds

of dynamical evolution [8]. The work is associated to the changes in the Hamiltonian, while the heat is associated to the change of the system state when the Hamiltonian is constant.

Since the system Hamiltonian changes only at time t_1, to measure the work we couple the system and the detector shortly before and after t_1 (Fig. 1).

In the present experiment, the (dissipative) dynamics of the system is given by the operator $U_{\rm diss} = R_z U_z R_x U_x$. The evolution generated by the latter operator can be divided into two parts, $R_x U_x$ and $R_z U_z$, where the system Hamiltonian can be considered constant. Before and after the time t_1, when the Hamiltonian is constant, the change in the system energy can be associated to the action of the environment and, thus, interpreted as dissipated heat. Analogously, we follow the scheme in Fig. 1 to store information about the dissipated heat in the σ_x and σ_z system basis, respectively. Note that with this coupling scheme, we obtain information about the heat, i.e., the dissipated energy, supplied *to the environment* (see the Supplemental Material [23]). If we are interested in the variation of the internal energy of the system, we need to couple the system and the detector at the beginning and at the end of the evolution only (see Fig. 1).

We would like to stress that the separation between the unitary and dissipative dynamics, i.e., between the interval in which the work is done and the heat is dissipated, has the only purpose of simplifying the discussion and the implementation on the NISQ device. As discussed in Ref. [9], the approach also works in more complex situations. The only constraint is that we must be able to couple the system and the detector on timescale Δt such that $\Delta t \ll \mathcal{T}$. Under this condition, in a single interval, the system Hamiltonian can be considered constant and the the system dynamics (if present) is associated to the effect of the environment and to the dissipated heat.

Coming back to the discussed case, the physical observable measured in the experiments is the phase accumulated in the detector using the different schemes. For a given system-detector coupling strength χ, it reads [9,21,30]

$$\mathcal{G}_{\chi,\mathcal{F}} = \frac{{}_D\langle 0|\rho_D(\mathcal{T})|1\rangle_D}{{}_D\langle 0|\rho_D^0|1\rangle_D} = \mathrm{Tr}_{S,E}\left[\mathcal{U}_{\chi,\mathcal{F}}\rho_S^0\mathcal{U}_{-\chi,\mathcal{F}}^\dagger\right], \quad (2)$$

where $\mathcal{F} = \Delta U, W, Q$, $\rho(\mathcal{T})$, $\rho_S(\mathcal{T}) = \mathrm{Tr}_{D,E}[\rho(\mathcal{T})]$, and $\rho_D(\mathcal{T}) = \mathrm{Tr}_{S,E}[\rho(\mathcal{T})]$ are the total, the final system, and the detector density operators, respectively; $\mathcal{U}_{\pm\chi,\mathcal{F}}$ represents the full (system, detector, and environments) evolution (see [9] and the Supplemental Material [23]).

By changing the system-detector coupling strength χ, we obtain the quasicharacteristic generating function (QCGF) that is related to quasimoments of the observable $\mathcal{F}$ [9,21,26,30]. In particular, the first derivative of $\mathcal{G}_{\chi,\mathcal{F}}$ with respect to χ gives the average value of $\mathcal{F}$. For example, by considering $\mathcal{F} = \Delta U$, i.e., the first coupling scheme in Fig. 1, by direct calculation, it can be shown that $d\mathcal{G}_{\chi,\Delta U}/d\chi|_{\chi=0} = \langle H_S(\mathcal{T}) - H_S(0)\rangle = \Delta U$ [9,21,26,30].

The Fourier transform of the QCGF allows us to obtain a quasiprobability distribution function: $\mathcal{P}(\mathcal{F}) = \int d\chi \mathcal{G}_{\chi,\mathcal{F}} e^{i\chi\mathcal{F}}$. By using the prefix "quasi," we stress that the above quantities are not obtained by direct physical measurements, but derived from the analysis of the detector phase measurements. Indeed, $\mathcal{P}(\mathcal{F})$ presents negative probability regions [9,31] that are related to the violation of the Leggett-Garg inequalities [9,25–28,31] and can therefore be seen as a signature of the quantum properties of the work.

III. RESULTS

The main results of the experiments on the IBMQ device are shown in Fig. 2 (see the Supplemental Material [23] for details about the implementation) for different dissipative parameters p. When no relaxation is present, i.e., $p = 0$, no heat is dissipated and the heat distributions are peaked around $Q = 0$. The internal energy and work QPDFs are identical and show the classical energy peaks at $\mathcal{E}/\epsilon = \pm 1, 0$. However, there are also quantum energy peaks at $\mathcal{E}/\epsilon = \pm 1/2$ corresponding to the exchange of half of an energy quantum, as predicted by the theory [9,21,30]. More importantly, in these regions, the probability density distribution can be negative, thus signaling a pure quantum effect related to the violation of the Leggett-Garg inequalities [9,25].

The experimental data and QPDFs are in excellent agreement with the theoretical predictions, which are presented as blue dots. The red dots represent the expected values obtained from a numerical simulation of the TMP, where the system energy is initially projectively measured. Clearly, the QPDFs not only contain all the information and reproduce the TMP distributions, but they allow us to determine the presence of additional quantum interference effects highlighted by the half-quantum energy exchanges [9,21].

For intermediate values of the system-environment coupling strength ($p = 0.5$ in Fig. 2), the QPDFs of W and ΔU have some notable differences, but the features described above persist. However, in this case, some heat is being dissipated by the system, as pointed out by the presence of a peak at energy $Q = \mathcal{E}/\epsilon = 1$. Notice that while the internal energy is bounded between ± 1, the dissipated heat is not. Because of the chosen dynamics, the system can dissipate energy at two times (formally when we apply R_x and R_y) corresponding to a maximum energy exchange of two energy quanta.

The strong dissipation case $p = 1$ has two interesting features. First, as expected, the peaks of the heat distribution are evidently signaling an increased dissipation. Second, the W and ΔU distributions are now both positively defined and no quantum energy exchange at $\mathcal{E}/\epsilon = \pm 1/2$ is present. The disappearance of the quantum region in the QPDFs signals the emergence of the classical limit due to the interaction of the system with an environment.

As a side remark, we note that the Q distribution is always classical, i.e., positively defined and with no half-quantum energy exchange. This is a feature we expect from a large Markovian environment that is always in equilibrium and, in this sense, a classical environment.

These results and trends are confirmed by the behavior of the average values shown in Fig. 3 as a function of the dissipative parameter p. The experimental points (in light blue) are in good agreement with the expected theoretical prediction (blue curve). For no or weak dissipation ($p = 0$ and $p = 0.5$), these are different from the one predicted by the TMP (red curve). The difference lies in the initial coherences and interference effects that are preserved with the present approach. For strong dissipation ($p = 1$), the averages

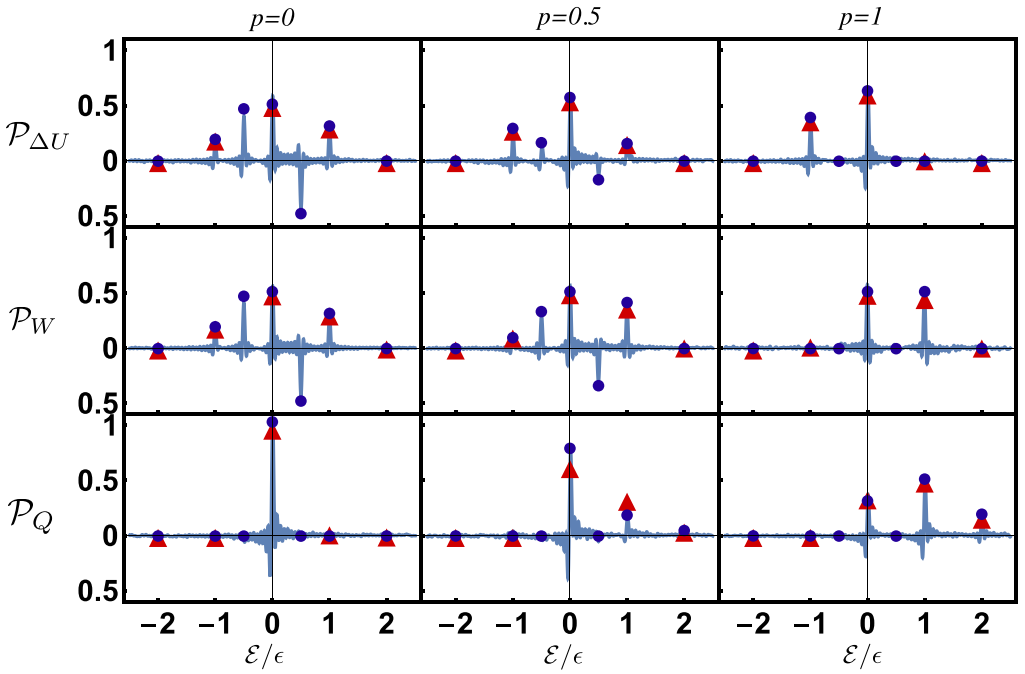

FIG. 2. The quasiprobability distribution functions for the variation of internal energy, work, and dissipated heat (y axis) with respect to the energy (x axis), normalized to the energy gap of the system, $\mathcal{E}/\epsilon$. The parameter p represents the strength of the dissipation from $p = 0$ (no dissipation) to $p = 1$ (full relaxation process). The blue dots represent the theoretical predictions of the discussed detection scheme. The red triangles represent the theoretical predictions of the two-measurement process. The quasiprobability distribution functions have been rescaled to plot them with the probability distribution obtained with the TMP (see the Supplemental Material [23]). In the experiments, we set $\theta = 0.7$, $\phi = 1.2$ for the initial state and $\alpha = 1$ and $\beta = 0.5$ for the system dynamics.

obtained with different approaches coincide. Since the main effects of a strong dissipation are to destroy the quantum coherences and make the evolution classical, this is another manifestation of the emergence of the classical limit that coincides with the TMP results.

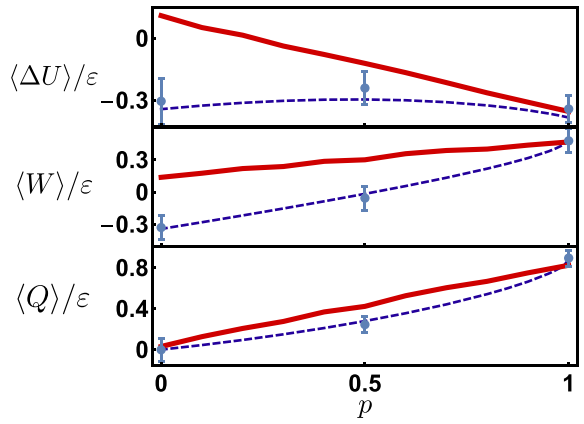

FIG. 3. The average values of the variation of internal energy, work, and dissipated heat normalized to ϵ as a function of the dissipative parameter p. The blue dots represent the experimental data with the corresponding error bars (see the Supplemental Material [23] for details). The dashed blue curve is the theoretical prediction of the discussed approach. The red solid curve is the prediction of the TMP obtained by simulations with the IBMQ computers. The error in these simulations is within the curve thickness. As can be seen, for strong dissipation, the three curves converge, demonstrating that the quantum features are destroyed and the classical limit is reached.

All the averages satisfy the energy conservation law $\langle\Delta U\rangle + \langle Q\rangle - \langle W\rangle = 0$. In particular, we find from the experimental data that the energy conservation law is satisfied within the experimental error (see the Supplemental Material [23]).

IV. CONCLUSIONS

The present approach has several advantages with respect to the one presented in Refs. [4,32]. First, it allows us to obtain the dissipated heat by acting on the system degrees of freedom. This is an important difference with respect to the theoretical proposal to measure the variation of the energy of the environment, which is practically unrealizable since it would require an insurmountable number of measurements. Other viable schemes have been designed in order to measure the dissipated energy quanta [12–16]. However, these can be used only in specific physical systems, while our scheme is system independent and, thus, can be used with any quantum system.

More importantly, the information about the classical TMP distributions is included in the more general QPDFs that, at the same time, contains much more valuable information about the quantumness of the process. In Wigner's spirit [24], these can be seen as quantum correction to an underlying classical process. The Wigner function has become an invaluable tool to understand quantum phenomena [33,34].

Analogously, the presented approach could shed light on the energy exchanges, allowing us to identify their quantum features. This is a first step toward understanding if and when quantum energy exchanges can be more efficient that classical ones and exploit their quantum advantage.

ACKNOWLEDGMENTS

The authors would like to thank E. De Vito, S. Gasparinetti, and A. Toigo for fruitful discussions. P.S. and N.Z. acknowledge financial support from INFN. The views expressed are those of the author and do not reflect the official policy or position of Q-CTRL.

[1] V. Giovannetti, S. Lloyd, and L. Maccone, Nat. Photon. **5**, 222 (2011).
[2] J. Aasi, J. Abadie, B. P. Abbott, R. Abbott, T. D. Abbott, M. R. Abernathy, C. Adams, T. Adams, P. Addesso, R. X. Adhikari *et al.*, Nat. Photon. **7**, 613 (2013).
[3] M. A. Nielsen and I. L. Chuang, *Quantum Computation and Quantum Information* (Cambridge University Press, Cambridge, 2010).
[4] M. Campisi, P. Hänggi, and P. Talkner, Rev. Mod. Phys. **83**, 771 (2011).
[5] P. Talkner, E. Lutz, and P. Hänggi, Phys. Rev. E **75**, 050102(R) (2007).
[6] R. Dorner, S. R. Clark, L. Heaney, R. Fazio, J. Goold, and V. Vedral, Phys. Rev. Lett. **110**, 230601 (2013).
[7] L. Mazzola, G. De Chiara, and M. Paternostro, Phys. Rev. Lett. **110**, 230602 (2013).
[8] P. Solinas, D. V. Averin, and J. P. Pekola, Phys. Rev. B **87**, 060508(R) (2013).
[9] P. Solinas and S. Gasparinetti, Phys. Rev. E **92**, 042150 (2015).
[10] M. Perarnau-Llobet, E. Bäumer, K. V. Hovhannisyan, M. Huber, and A. Acin, Phys. Rev. Lett. **118**, 070601 (2017).
[11] T. B. Batalhão, A. M. Souza, L. Mazzola, R. Auccaise, R. S. Sarthour, I. S. Oliveira, J. Goold, G. De Chiara, M. Paternostro, and R. M. Serra, Phys. Rev. Lett. **113**, 140601 (2014).
[12] J. Pekola, P. Solinas, A. Shnirman, and D. Averin, New J. Phys. **15**, 115006 (2013).
[13] S. Gasparinetti, K. L. Viisanen, O.-P. Saira, T. Faivre, M. Arzeo, M. Meschke, and J. P. Pekola, Phys. Rev. Appl. **3**, 014007 (2015).
[14] K. L. Viisanen, S. Suomela, S. Gasparinetti, O.-P. Saira, J. Ankerhold, and J. P. Pekola, New J. Phys. **17**, 055014 (2015).
[15] O.-P. Saira, M. Zgirski, K. L. Viisanen, D. S. Golubev, and J. P. Pekola, Phys. Rev. Appl. **6**, 024005 (2016).
[16] V. Vesterinen, O.-P. Saira, I. Räisänen, M. Möttönen, L. Grönberg, J. Pekola, and J. Hassel, Supercond. Sci. Technol. **30**, 085001 (2017).
[17] A. Ronzani, B. Karimi, J. Senior, Y.-C. Chang, J. T. Peltonen, C. Chen, and J. P. Pekola, Nat. Phys. **14**, 991 (2018).
[18] J. P. S. Peterson, T. B. Batalhão, M. Herrera, A. M. Souza, R. S. Sarthour, I. S. Oliveira, and R. M. Serra, Phys. Rev. Lett. **123**, 240601 (2019).
[19] B. Karimi, D. Nikolić, T. Tuukkanen, J. T. Peltonen, W. Belzig, and J. P. Pekola, Phys. Rev. Appl. **13**, 054001 (2020).
[20] B. Karimi, F. Brange, P. Samuelsson, and J. P. Pekola, Nat. Commun. **11**, 367 (2020).
[21] P. Solinas and S. Gasparinetti, Phys. Rev. A **94**, 052103 (2016).
[22] Ibm quantum experience https://quantum-computing.ibm.com/ (unpublished).
[23] See Supplemental Material at http://link.aps.org/supplemental/10.1103/PhysRevA.103.L060202 for details about the implementation on IBM quantum computers, the environment engineering and data analysis.
[24] E. Wigner, Phys. Rev. **40**, 749 (1932).
[25] A. J. Leggett and A. Garg, Phys. Rev. Lett. **54**, 857 (1985).
[26] A. A. Clerk, Phys. Rev. A **84**, 043824 (2011).
[27] M. Lostaglio, Phys. Rev. Lett. **120**, 040602 (2018).
[28] A. Levy and M. Lostaglio, PRX Quantum **1**, 010309 (2020).
[29] G. García-Pérez, M. A. C. Rossi, and S. Maniscalco, npj Quantum Inf. **6**, 1 (2020).
[30] P. Solinas, H. J. D. Miller, and J. Anders, Phys. Rev. A **96**, 052115 (2017).
[31] P. P. Hofer and A. A. Clerk, Phys. Rev. Lett. **116**, 013603 (2016).
[32] S. Gasparinetti, P. Solinas, A. Braggio, and M. Sassetti, New J. Phys. **16**, 115001 (2014).
[33] P. Bertet, A. Auffeves, P. Maioli, S. Osnaghi, T. Meunier, M. Brune, J. M. Raimond, and S. Haroche, Phys. Rev. Lett. **89**, 200402 (2002).
[34] S. Deléglise, I. Dotsenko, C. Sayrin, J. Bernu, M. Brune, J.-M. Raimond, and S. Haroche, Nature (London) **455**, 510 (2008).